New Spin on LIGO-Virgo Binary Black Holes

Sylvia Biscoveanu, Maximiliano Isi, Salvatore Vitale, and Vijay Varma

Phys. Rev. Lett. **126**, 171103 — Published 29 April 2021

DOI: 10.1103/PhysRevLett.126.171103

A new spin on LIGO-Virgo binary black holes

Sylvia Biscoveanu,[1,2,*] Maximiliano Isi,[1,2,†] Salvatore Vitale,[1,2] and Vijay Varma[3,4,‡]

[1] *LIGO Laboratory, Massachusetts Institute of Technology, Cambridge, Massachusetts 02139, USA*
[2] *Department of Physics and Kavli Institute for Astrophysics and Space Research, Massachusetts Institute of Technology, 77 Massachusetts Ave, Cambridge, MA 02139, USA*
[3] *TAPIR, California Institute of Technology, Pasadena, CA 91125, USA*
[4] *Department of Physics, and Cornell Center for Astrophysics and Planetary Science, Cornell University, Ithaca, New York 14853, USA*

(Dated: March 5, 2021)

Gravitational waves from binary black holes have the potential to yield information on both of the intrinsic parameters that characterize the compact objects: their masses and spins. While the component masses are usually resolvable, the component spins have proven difficult to measure. This limitation stems in great part from our choice to inquire about the spins of the most and least massive objects in each binary, a question that becomes ill-defined when the masses are equal. In this paper we show that one can ask a different question of the data: what are the spins of the objects with the highest and lowest dimensionless spins in the binary? We show that this can significantly improve estimates of the individual spins, especially for binary systems with comparable masses. When applying this parameterization to the first 13 gravitational-wave events detected by the LIGO-Virgo collaboration (LVC), we find that the highest-spinning object is constrained to have nonzero spin for most sources and to have significant support at the Kerr limit for GW151226 and GW170729. A joint analysis of all the confident binary black hole detections by the LVC finds that, unlike with the traditional parametrization, the distribution of spin magnitude for the highest-spinning object has negligible support at zero spin. Regardless of the parameterization used, the configuration where all of the spins in the population are aligned with the orbital angular momentum is excluded from the 90% credible interval for the first ten events and from the 99% credible interval for all current confident detections.

Introduction. Gravitational waves from compact binary coalescences (CBCs) carry imprints of the spin angular momenta $\vec{S}$ of the black holes (BHs) or neutron stars (NSs) that originated them. The Advanced LIGO [1] and Virgo [2] detectors can extract this information to obtain key insights about the astrophysics of compact binaries; because the magnitude and orientation of the spins reflect the system's history, such a measurement could reveal the binary's formation mechanism [3, 4]. For instance, we expect the spins of compact binaries formed in isolation to be preferentially aligned with the orbital angular momentum $\vec{L}$ [5–14], while the same is not true of binaries formed dynamically [12, 15–19]. Identifying the formation channel of compact binaries is one of the most pressing open problems in astrophysics, making the measurement of component spins a high-value target.

Unfortunately, the ability to measure individual spins with the LIGO and Virgo detectors has been limited, since little information about these quantities is imprinted in the inspiral waveform at leading order [20–23]. At the population level, current inferences on the black hole spin distribution indicate that most sources have low spin magnitudes when considering the distributions of both the individual component spins [24, 25] and of the spin components aligned with [26–29] and perpendicular to [30] the orbital angular momentum. In this paper, we show that we can draw clearer conclusions about the spins of individual objects by using a more suitable basis. Rather than attempting to identify the spin of the heaviest and lightest of the two objects, as is usually done, we infer the properties of the objects with the highest and lowest dimensionless spin. This straightforward reparametrization of the problem can cast a new light on the component spin measurements for near-equal-mass binaries, which appear to be the majority [24, 28, 31]. In the following, we present our proposed reparametrization and demonstrate its impact both on simulated signals and on actual LIGO-Virgo detections.

Approach. Within general relativity, a CBC signal is fully determined by a set of parameters encoding the intrinsic properties of the binary as well as extrinsic parameters specifying its distance and orientation. The intrinsic parameters correspond to the mass m_i and dimensionless spin $\vec{\chi}_i = \vec{S}_i c/(Gm^2)$ of each component object $i \in \{1, 2\}$, plus additional quantities incorporating matter effects and eccentricity. Virtually all of the literature, including LIGO-Virgo collaboration papers [32–35], labels the compact objects with respect to their mass, with the index 1 corresponding to the heaviest of the two objects and 2 to the lightest, $m_1 \geq m_2$. However, this choice is suboptimal for systems with similar masses, as it becomes degenerate for $m_1 = m_2$. In that limit, the standard mass-based sorting induces undesired structure in the posteriors for the spin parameters.[36]

To avoid these degeneracies, we instead propose to identify objects by their dimensionless spin magnitude $\chi = |\vec{\chi}|$, and define an equivalent set of quantities m_j and $\vec{\chi}_j$ for $j \in \{A, B\}$, with A referring to the object with

TABLE I. Comparison of the maximum posterior value with uncertainty quoted at the 90% level and the credible level at which the true value is recovered ($\mathrm{CL_{inj}}$) for the component mass and spin parameters using both the mass and spin sorting for the simulated signal. The credible level is calculated using the highest posterior density method.

Parameter	Inj.	Mass sorting		Spin sorting	
		maxP	$\mathrm{CL_{inj}}$	maxP	$\mathrm{CL_{inj}}$
$m_{1/A}$	40 $M_\odot$	$40.90^{+3.02}_{-1.43}$	58.5%	$39.27^{+3.77}_{-2.88}$	45.7%
$m_{2/B}$	40 $M_\odot$	$38.70^{+1.74}_{-2.38}$	67.2%	$40.19^{+3.05}_{-3.05}$	0%
$\chi_{1/A}$	0.8	$0.01^{+0.85}_{-0.01}$	87.1%	$0.77^{+0.21}_{-0.17}$	11.5%
$\chi_{2/B}$	0	$0.80^{+0.19}_{-0.80}$	61.4%	$0.01^{+0.41}_{-0.01}$	0%
$\theta_{1/A}$	1.57 rad	$1.54^{+0.87}_{-0.80}$	0%	$1.59^{+0.29}_{-0.34}$	0%
$\theta_{2/B}$	–	$1.62^{+0.73}_{-0.58}$	–	$1.54^{+1.20}_{-0.81}$	–

the highest spin and B to the lowest, $\chi_A \geq \chi_B$. (In the equal-mass limit, sorting by dimensionless spin is equivalent to sorting by the component angular momenta, $\vec{S}_i$.) This amounts to a coordinate transformation effecting $\chi_A = \max(\chi_1, \chi_2)$ and $\chi_B = \min(\chi_1, \chi_2)$. The mass of the highest-χ component is m_A, just as χ_1 is the spin magnitude of the highest-m component. In the following, we will refer to the usual $\{1, 2\}$ parametrization as *mass sorting*, and to the new $\{A, B\}$ parameterization as *spin sorting*.

Simulated signal. Before we apply the spin sorting to real detections, we perform Bayesian parameter estimation on a simulated equal-mass binary BH (BBH) system with $\chi_A = 0.8$ and $\chi_B = 0$ to demonstrate the resolving power of the new parameterization. The system has a redshifted total mass of 80 $M_\odot$, and is oriented nearly edge-on with an inclination angle $\theta_{JN} = 80.21°$. The luminosity distance, $d_L = 831.47$ Mpc, is chosen so that the signal is recovered with a network signal-to-noise ratio (SNR) of 30 by the two advanced LIGO instruments plus advanced Virgo, all operating at design sensitivity [1, 2]. The tilt of the spinning object is $\theta_A = 90°$ with respect to the orbital angular momentum, meaning that the spin vector lies entirely in the orbital plane.

We assume standard priors for LIGO-Virgo analyses [33, 37]; these imply a disjoint uniform prior on m_A and m_B, and a uniform two-dimensional prior on χ_A, χ_B. As is the case for m_1 and m_2, the definition $\chi_A > \chi_B$ results in a "triangular" marginal prior for χ_A and χ_B, i.e. a probability density linearly increasing and decreasing, respectively, with the quantity (black histograms in Fig. 1). In order to isolate the effect of the chosen parameterization on the recovered posteriors, we do not add noise to the simulated data [38].

In Fig. 1, we compare the resulting measurements of the spin magnitudes and tilts using both the mass and spin sortings. The mass sorting induces a bimodal posterior in the χ_1, χ_2 plane (symmetric around $\chi_1 = \chi_2$), showing

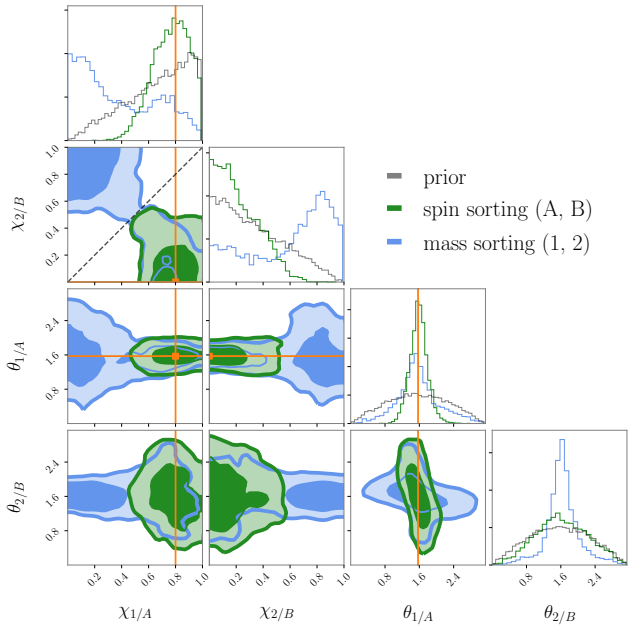

FIG. 1. Comparison corner plot showing the spin magnitudes and tilts recovered for our simulated equal-mass signal using both the mass sorting in green and the spin sorting in blue. The marginalized one-dimensional priors for the spin sorting are shown in grey. Orange lines mark the true value, and the equal-spin diagonal is shown as a dashed line for reference.

that a high spin could be assigned to either component, while the marginal posteriors on χ_1 and χ_2 are largely unconstrained. The spin sorting breaks this degeneracy, restricting the posterior so that χ_A peaks at the true value and χ_B rails against the lower edge of the prior. A similar degeneracy can be seen in the two-dimensional posterior for θ_1 and θ_2 in the mass sorting, which shows that information is retrieved for the tilt of one of the two objects without identifying which. Switching to the spin sorting, the θ_A posterior is well-constrained, while θ_B returns the prior. Thus, this parametrization makes it clear that we can measure the tilt of the highest-spin object but cannot say anything about the lowest-spin one, as expected given that $\chi_B = 0$, making θ_B irrelevant. In Table I, we show the maximum posterior probability values and associated 90% credible interval for the component masses, spins, and tilt angles obtained using both parameterizations. We also show the credible level at which the true value is recovered. The mass ratio posterior is peaked narrowly around the equal-mass limit, $q = 0.996^{+0.004}_{-0.138}$. The statistical uncertainty for the component masses m_A and m_B is greater than for m_1 and m_2 because there is no imposed ordering on m_A and m_B.

In order to verify that the improved resolution of the spin sorting is robust against changes in the true spin magnitude and tilt and that it extends to systems without exactly equal component masses, we repeat our simula-

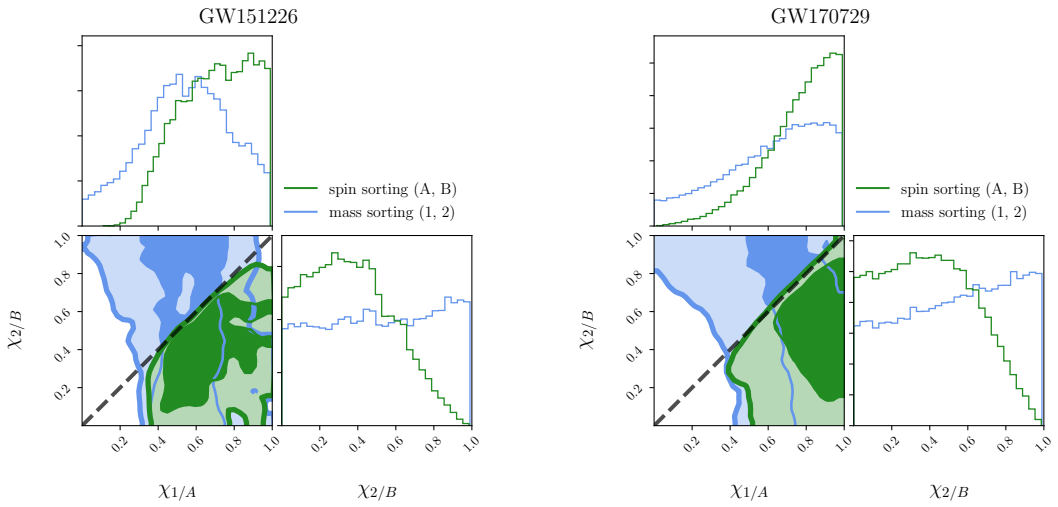

FIG. 2. Comparison corner plot for the spin magnitudes for the posteriors obtained using the IMRPhenomPv2 waveform for GW151226 and GW170729. The equal-spin diagonal is shown as a dashed line for reference.

tion for a variety of different binary parameters. We find a similar improvement in the resolution of the component spins for systems with lower spins, $\chi_A = 0.2$, with an aligned primary spin, $\theta_A = 0$, and with slightly unequal mass ratios, $q = m_2/m_1 = 0.9$, when each of these parameters is varied independently in simulated signals with the same SNR as the original. When the network SNR is decreased to 12, the component spins cannot be well-measured using either parameterization, meaning that only minor deviations from the priors are observed.

The spin sorting ceases to be useful for systems where the mass ratio is measurably different from unity. Looking at a system with $q = 0.7$ and SNR $= 30$, the spin sorting introduces the same type of degeneracies in the spin parameters as are present in Fig. 1 under the mass sorting. This is because the spin of the most massive object is well-defined for systems where the most massive object can be distinguished. Systems with equal spin magnitudes—both nonspinning and highly spinning with $\chi_1 = \chi_2 = 0.8$—similarly do not benefit from the spin sorting, as the spin magnitude posteriors are largely unchanged in this case. (The χ_A posterior for the nonspinning injection peaks at $\chi_A = 0$, even though this region is disfavored by the prior.) However, when analyzing a system with $\chi_1 = \chi_2 = 0.8$ and unequal tilt angles, $\theta_1 = \pi/2$ and $\theta_2 = 0$, the bimodality in the tilt posterior can be resolved by instead sorting by the tilt angles without affecting the spin magnitude posteriors.

LIGO-Virgo detections. We apply the same reparameterization to the publicly released posterior samples for the first 13 LIGO-Virgo detections [32–35, 39]. The ten BBH mergers announced in the first LIGO-Virgo catalog (GWTC-1) are all consistent with $q = 1$, although the posteriors all support considerably lower values than the simulated signal in Fig. 1. For these systems, we find that the differences between the spin and mass sorting are generally not as significant as for the simulation. This is consistent with the results of the low-SNR simulation discussed above.

For the two events whose posteriors in the mass sorting already indicated a preference for non-zero spins, GW151226 [40] and GW170729 [41], $\chi_A = 0$ is ruled out with 3σ credibility. For GW170729, $\chi_A = \chi_B = 1$ is included within the 90% credible region, while for GW151226, $\chi_A = 1$ is included in the 50% credible region as long as $0.5 < \chi_B < 0.7$. We show spin magnitude posteriors for these events using both parameterizations in Fig. 2. For all the BBH systems analyzed, the lower bound of the 90% credible interval for the χ_A posterior is $\chi_A \geq 0.14$, although this is dominated by the triangular prior (grey line in Fig. 1). On the other hand, the χ_1 posterior is only constrained to $\chi_1 > 0.14$ for GW151226 and GW170729 under the mass sorting. For the unequal-mass binary GW190412 [35], the spin sorting introduces degeneracies in the spin parameters that were not present in the mass-based sorting, which we expected from our $q < 1$ simulations. In the Supplementary Material, we explore the features of the posteriors for GW190412 and the two binary NS systems and show that waveform systematics proved to be important for some events (including GW150914).

Population analyses. In order to determine the effects of the spin sorting on the inferred population properties of BH spins, we use the infrastructure of hierarchical Bayesian inference to characterize the underlying distributions of χ_A and χ_B. If the mass-sorted spin magnitudes for individual events, $\chi_{1/2}$, are modeled as being drawn from the same Beta distribution following [24, 42], we can compute the corresponding χ_A and χ_B distributions using order statistics, by assuming they correspond to

the maximum and minimum of two draws from the $\chi_{1/2}$ distribution. We use the publicly released posterior samples for the $\chi_{1/2}$ hyperparameters from LVC analyses first including only GWTC-1 events [24, 43], then including all 44 confident BBH detections reported in GWTC-2 [44–46]. We present our results using the posterior population distribution (PPD), which is the expected distribution for the individual-event parameters of new BBH events inferred from the accumulated set of detections (e.g., [24], see Supplementary Material).

In Figure 3 we show the PPDs for $p(\chi_A)$ and $p(\chi_B)$ as well as the 50% and 90% credible bands. The inferred distribution for χ_A (top) peaks at around $\chi_A \sim 0.3$ and has negligible support for $p(\chi_A) = 0$ for both the GWTC-1 and GWTC-2 analyses, indicating that most of the highest-spinning BHs in LIGO-Virgo binaries have nonzero spins. This is very different from the distribution inferred for the mass sorted spins, $p(\chi_{1/2})$, which has considerable support at $\chi_{1/2} = 0$ (see Fig. 8 of [24] and Fig. 10 of [45]). The lower bound of the 50% credible interval for $p(\chi_A)$ is $\chi_A = 0.19$, while the 50% credible interval for $\chi_{1/2}$ extends down to $\chi_{1/2} = 0.06$ for the GWTC-2 analysis. The distribution of spin magnitudes for the lowest-spinning BHs (bottom) is consistent with peaking at $\chi_B = 0$ for both analyses and has more posterior support at $\chi_B = 0$ when including the full GWTC-2 sample. All these distributions vary significantly from those obtained using samples from the spin magnitude prior instead of posterior samples for the 44 confident BBH detections from GWTC-2 (dashed lines in Fig. 3).

For the spin tilt angles, we follow [24, 47] and model the distribution as the sum of two populations motivated by the most popular BBH formation channels (eg. [6, 8, 12, 48]): an isotropic component and a preferentially aligned component, where the hyperparameters $\sigma_{1/A}$ and $\sigma_{2/B}$ control the spread in the possible tilt angles around $\theta_{1/A} = \theta_{2/B} = 0$. A nonzero value for σ indicates that not all tilts are aligned. We conduct hierarchical Bayesian inference using this model for the tilt angles under both the mass and spin sorting. In Fig. 4, we show the posteriors on the hyperparameters describing the spin tilt population model for the 44 confident BBH detections in GWTC-2. The blue distribution corresponds to inference starting from the mass-sorted single-event posteriors, while the green distribution shows the same for the spin-sorted posteriors. The posterior for σ_A is constrained slightly further away from 0 than that of σ_1, while the opposite is true for σ_B and σ_2. This indicates that the posterior information gain relative to the prior is less balanced between the two tilt angles in the spin sorting than the mass sorting.

We highlight that $\sigma_{1/A} = \sigma_{2/B} = 0$ is excluded with $> 99\%$ credibility for both parameterizations when marginalized over spin magnitude. The same is true at 90% credibility when considering only the GWTC-1 events. This means that the preferentially aligned component is more likely to have nonzero width, and hence a

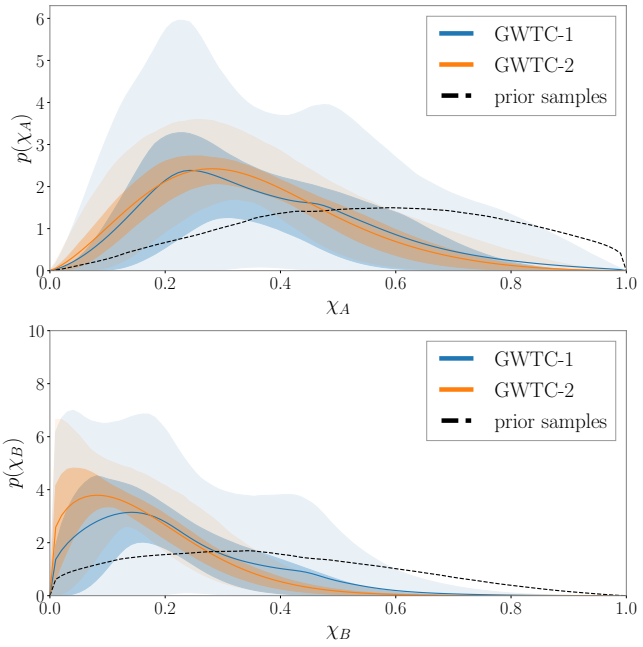

FIG. 3. PPDs for $p(\chi_A)$ (top) and $p(\chi_B)$ (bottom). The blue curves include only events from GWTC-1, while the orange curves include all 44 confident BBH events in GWTC-2. The shaded regions correspond to the 50% and 90% credible intervals, and the PPDs obtained using prior samples for the individual GWTC-2 events are shown in the dashed lines.

fraction of binaries is likely to have in-plane spin components. This result agrees with previous analyses, which find that a fully-aligned population is disfavored by the LVC detections reported in GWTC-1 [24, 27, 49], and that the current detections are consistent with a population of high spins that are significantly misaligned with respect to the orbital angular momentum. [26, 29]. The GWTC-2 results agree with those presented in [45] using two different spin tilt parameterizations from the one we use, which find evidence for general-relativistic spin precession at the population level. We confirm that this feature originates in the data—and is not just an artifact of the Monte Carlo integration performed during hierarchical inference step—by replacing the mass-sorted spin tilt posteriors from individual events with draws from the prior. This results in an uninformative distribution for σ_1, σ_2 consistent with having uniform support across the prior range, including the region around $\sigma_1 = \sigma_2 = 0$ (shown in grey in Fig. 4). The region $\sigma_{1/A}, \sigma_{2/B} \geq 1.6$ is also excluded at $> 90\%$ credibility, indicating that a fully isotropic spin distribution corresponding to high values of σ is statistically disfavored. Additional analysis details are provided in the Supplementary Material.

Conclusion. We have demonstrated the advantages of introducing an alternative labeling for the component objects of a compact binary based on the spins instead of the masses; we denote the object with the largest

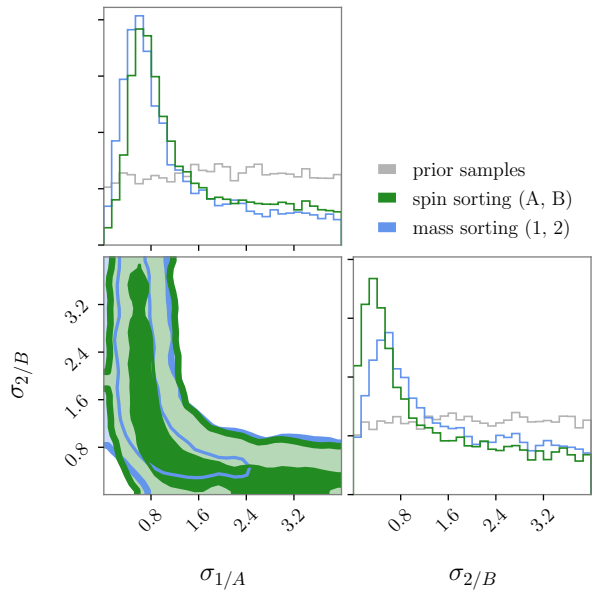

FIG. 4. Corner plot comparing the inference on the spin tilt hyperparameters using the mass sorted tilts θ_1 and θ_2 to the posteriors obtained using the same population model but for the spin sorted tilts θ_A and θ_B for the GWTC-2 events. The posteriors obtained using prior samples for the individual events are shown in grey.

(smallest) spin magnitude by A (B), such that $\chi_A > \chi_B$. Through analysis of simulated signals, we find that this sorting improves the resolution of the component spins of binaries consistent with having equal mass, regardless of the magnitude and tilt of the primary spin. When applied to the posteriors for the GWTC-1 events, we find that the most-spinning object is consistent with having extremal spin for the events that were already known to prefer nonzero spins, GW151226 and GW170729. The spin sorting ceases to be useful for systems with measurably unequal masses, as was the case for GW190412.

We characterize the distributions of $\chi_A, \chi_B, \theta_A, \theta_B$ of the 44 confident GWTC-2 BBH events by means of hierarchical Bayesian inference. Modeling the mass-sorted spins as drawn from a Beta distribution, we compute the implied probability densities for χ_A and χ_B and find that $p(\chi_A)$ peaks at $\chi_A \sim 0.3$ and has negligible support at $\chi_A = 0$, while $p(\chi_B)$ and $p(\chi_{1/2})$ have considerable posterior support at $\chi = 0$. We thus conclude, at the population level, that most of the BBHs detected by LIGO-Virgo have at least one component with nonzero spin. When modeling the distributions of spin tilt angles, we find that the configuration where all of the spins in the population are aligned with the orbital angular momentum is excluded from the 99% credible interval for both the mass and the spin sorting.

We end by stressing that the spin sorting does not introduce new information into the analysis. We are not applying different priors, but rather defining a new set of parameters that can be inferred using the same individual-event posterior samples used in the original mass-sorting. This implies that the Bayesian evidence of the data is unchanged. The reparameterization can be done entirely in post-processing and does not affect the posteriors for parameters that do not distinguish between the binary components like the effective aligned and precessing spins, $\chi_{\rm eff}$ and $\chi_{\rm p}$. The spin sorting also does not change existing population-level inferences obtained from the mass-sorted component parameters, with the possible exception of analyses relying on marginalized one-dimensional posteriors on the component spin quantities, which cannot encode the parameter degeneracies that we noted for signals consistent with $q \approx 1$. While in some cases BBH formation channels make it more natural to label the component objects based on their mass, thinking about the objects primarily in terms of spin could lead to rich new ways to test astrophysical models moving forward [50].

Acknowledgments. S.B., M.I. and S.V. acknowledge support of the National Science Foundation and the LIGO Laboratory. LIGO was constructed by the California Institute of Technology and Massachusetts Institute of Technology with funding from the National Science Foundation and operates under cooperative agreement PHY-0757058. S.B. is also supported by the Paul and Daisy Soros Fellowship for New Americans and the NSF Graduate Research Fellowship under Grant No. DGE-1122374. M.I. is supported by NASA through the NASA Hubble Fellowship grant No. HST-HF2-51410.001-A awarded by the Space Telescope Science Institute, which is operated by the Association of Universities for Research in Astronomy, Inc., for NASA, under contract NAS5-26555. V.V. is generously supported by the Sherman Fairchild Foundation, and NSF grants PHY–170212 and PHY–1708213 at Caltech, and by a Klarman Fellowship at Cornell. The authors would like to thank Colm Talbot for help with `GWPopulation`, and Thomas Callister, Thomas Dent, Maya Fishbach, and Eric Thrane for careful comments on the manuscript. We also thank Will Farr, Katerina Chatziioannou, Javier Roulet, Leo Stein, Simona Miller, Carl-Johan Haster, Saavik Ford, Barry McKernan, Daniel Wysocki, Richard O'Shaughnessy, and others for useful discussions. This paper carries LIGO document number LIGO-P2000247.

* sbisco@mit.edu
† NHFP Einstein fellow
‡ Klarman fellow

[1] J. Aasi *et al.* (LIGO Scientific), Class. Quant. Grav. **32**, 074001 (2015), arXiv:1411.4547 [gr-qc].
[2] F. Acernese *et al.* (VIRGO), Class. Quant. Grav. **32**, 024001 (2015), arXiv:1408.3978 [gr-qc].

[3] D. Gerosa, M. Kesden, E. Berti, R. O'Shaughnessy, and U. Sperhake, Phys. Rev. D **87**, 104028 (2013), arXiv:1302.4442 [gr-qc].
[4] D. Gerosa, E. Berti, R. O'Shaughnessy, K. Belczynski, M. Kesden, D. Wysocki, and W. Gladysz, Phys. Rev. D **98**, 084036 (2018), arXiv:1808.02491 [astro-ph.HE].
[5] A. V. Tutukov and L. R. YungelSon, Mon. Not. Roy. Astron. Soc. **260**, 675 (1993).
[6] V. Kalogera, Astrophys. J. **541**, 319 (2000), arXiv:astro-ph/9911417.
[7] P. Grandclement, M. Ihm, V. Kalogera, and K. Belczynski, Phys. Rev. D **69**, 102002 (2004), arXiv:gr-qc/0312084.
[8] K. A. Postnov and L. R. Yungelson, Living Rev. Rel. **17**, 3 (2014), arXiv:1403.4754 [astro-ph.HE].
[9] K. Belczynski, D. E. Holz, T. Bulik, and R. O'Shaughnessy, Nature **534**, 512 (2016), arXiv:1602.04531 [astro-ph.HE].
[10] I. Mandel and S. E. de Mink, Mon. Not. Roy. Astron. Soc. **458**, 2634 (2016), arXiv:1601.00007 [astro-ph.HE].
[11] Marchant, Pablo, Langer, Norbert, Podsiadlowski, Philipp, Tauris, Thomas M., and Moriya, Takashi J., A&A **588**, A50 (2016).
[12] C. L. Rodriguez, M. Zevin, C. Pankow, V. Kalogera, and F. A. Rasio, Astrophys. J. Lett. **832**, L2 (2016), arXiv:1609.05916 [astro-ph.HE].
[13] R. O'Shaughnessy, D. Gerosa, and D. Wysocki, Phys. Rev. Lett. **119**, 011101 (2017), arXiv:1704.03879 [astro-ph.HE].
[14] S. Stevenson, A. Vigna-Gómez, I. Mandel, J. W. Barrett, C. J. Neijssel, D. Perkins, and S. E. de Mink, Nature Commun. **8**, 14906 (2017), arXiv:1704.01352 [astro-ph.HE].
[15] S. Sigurdsson and L. Hernquist, Nature **364**, 423 (1993).
[16] M. Miller and V. M. Lauburg, Astrophys. J. **692**, 917 (2009), arXiv:0804.2783 [astro-ph].
[17] I. Mandel and R. O'Shaughnessy, Class. Quant. Grav. **27**, 114007 (2010), arXiv:0912.1074 [astro-ph.HE].
[18] S. Portegies Zwart, S. McMillan, and M. Gieles, Ann. Rev. Astron. Astrophys. **48**, 431 (2010), arXiv:1002.1961 [astro-ph.GA].
[19] M. J. Benacquista and J. M. Downing, Living Rev. Rel. **16**, 4 (2013), arXiv:1110.4423 [astro-ph.SR].
[20] T. Damour, Phys. Rev. D **64**, 124013 (2001).
[21] E. Racine, Phys. Rev. D **78**, 044021 (2008), arXiv:0803.1820 [gr-qc].
[22] P. Ajith, M. Hannam, S. Husa, Y. Chen, B. Brügmann, N. Dorband, D. Müller, F. Ohme, D. Pollney, C. Reisswig, L. Santamaría, and J. Seiler, Phys. Rev. Lett. **106**, 241101 (2011).
[23] K. K. Ng, S. Vitale, A. Zimmerman, K. Chatziioannou, D. Gerosa, and C.-J. Haster, Phys. Rev. D **98**, 083007 (2018), arXiv:1805.03046 [gr-qc].
[24] B. Abbott *et al.* (LIGO Scientific, Virgo), Astrophys. J. Lett. **882**, L24 (2019), arXiv:1811.12940 [astro-ph.HE].
[25] C. Kimball, C. Talbot, C. P. Berry, M. Carney, M. Zevin, E. Thrane, and V. Kalogera, (2020), arXiv:2005.00023 [astro-ph.HE].
[26] W. M. Farr, S. Stevenson, M. Coleman Miller, I. Mandel, B. Farr, and A. Vecchio, Nature **548**, 426 (2017), arXiv:1706.01385 [astro-ph.HE].
[27] V. Tiwari, S. Fairhurst, and M. Hannam, Astrophys. J. **868**, 140 (2018), arXiv:1809.01401 [gr-qc].
[28] J. Roulet and M. Zaldarriaga, Mon. Not. Roy. Astron. Soc. **484**, 4216 (2019), arXiv:1806.10610 [astro-ph.HE].
[29] S. Miller, T. A. Callister, and W. Farr, Astrophys. J. **895**, 128 (2020), arXiv:2001.06051 [astro-ph.HE].
[30] S. Fairhurst, R. Green, M. Hannam, and C. Hoy, Phys. Rev. D **102**, 041302 (2020), arXiv:1908.00555 [gr-qc].
[31] M. Fishbach and D. E. Holz, Astrophys. J. Lett. **891**, L27 (2020), arXiv:1905.12669 [astro-ph.HE].
[32] R. Abbott *et al.* (LIGO Scientific, Virgo), (2019), arXiv:1912.11716 [gr-qc].
[33] B. Abbott *et al.* (LIGO Scientific, Virgo), Phys. Rev. X **9**, 031040 (2019), arXiv:1811.12907 [astro-ph.HE].
[34] B. Abbott *et al.* (LIGO Scientific, Virgo), Astrophys. J. Lett. **892**, L3 (2020), arXiv:2001.01761 [astro-ph.HE].
[35] R. Abbott *et al.* (LIGO Scientific, Virgo), Phys. Rev. D **102**, 043015 (2020), arXiv:2004.08342 [astro-ph.HE].
[36] Assuming a universal equation of state, tidal parameters for binary NSs should be unaffected, since the least massive object should be the most deformable.
[37] J. Veitch *et al.*, Phys. Rev. **D91**, 042003 (2015), arXiv:1409.7215 [gr-qc].
[38] M. Vallisneri, Phys. Rev. D **77**, 042001 (2008), arXiv:gr-qc/0703086.
[39] M. Vallisneri, J. Kanner, R. Williams, A. Weinstein, and B. Stephens, J. Phys. Conf. Ser. **610**, 012021 (2015), arXiv:1410.4839 [gr-qc].
[40] B. P. Abbott *et al.* (LIGO Scientific, Virgo), Phys. Rev. Lett. **116**, 241103 (2016), arXiv:1606.04855 [gr-qc].
[41] K. Chatziioannou *et al.*, Phys. Rev. D **100**, 104015 (2019), arXiv:1903.06742 [gr-qc].
[42] D. Wysocki, J. Lange, and R. O'Shaughnessy, Phys. Rev. D **100**, 043012 (2019).
[43] B. Abbott *et al.*, "Full data release for "binary black hole population properties inferred from the first and second observing runs of advanced ligo and advanced virgo"," (2020).
[44] R. Abbott *et al.* (LIGO Scientific, Virgo), (2020), arXiv:2010.14527 [gr-qc].
[45] R. Abbott *et al.* (LIGO Scientific, Virgo), (2020), arXiv:2010.14533 [astro-ph.HE].
[46] B. Abbott *et al.*, "Data release for "population properties of compact objects from the second ligo-virgo gravitational-wave transient catalog"," (2020).
[47] C. Talbot and E. Thrane, Phys. Rev. D **96**, 023012 (2017), arXiv:1704.08370 [astro-ph.HE].
[48] J. D. Schnittman, Phys. Rev. D **70**, 124020 (2004).
[49] D. Wysocki, J. Lange, and R. O'Shaughnessy, Phys. Rev. D **100**, 043012 (2019).
[50] The Supplementary Material contains more details on the Bayesian methods employed for both the individual-event analyses and the hierarchical inference, as well as additional information for the features of the posteriors of GW190412, the two binary NS systems, and an exploration of the effect of waveform systematics. This further includes Refs. [51–72].
[51] J. D. Romano and N. J. Cornish, Living Rev. Rel. **20**, 2 (2017), arXiv:1608.06889 [gr-qc].
[52] V. Varma, S. E. Field, M. A. Scheel, J. Blackman, D. Gerosa, L. C. Stein, L. E. Kidder, and H. P. Pfeiffer, Phys. Rev. Research. **1**, 033015 (2019), arXiv:1905.09300 [gr-qc].
[53] C. Talbot and E. Thrane, Astrophys. J. **856**, 173 (2018), arXiv:1801.02699 [astro-ph.HE].
[54] T. J. Loredo, in *Bayesian Inference and Maximum Entropy Methods in Science and Engineering ed R. Fischer, R. Preuss and U. V. Toussaint*, AIP Conference Series, Vol. 735 (AIP, Melville, NY, 2004) p. 195.

[55] M. Fishbach, D. E. Holz, and W. M. Farr, Astrophys. J. Lett. **863**, L41 (2018).

[56] E. Thrane and C. Talbot, Publ. Astron. Soc. Austral. **36**, e010 (2019), arXiv:1809.02293 [astro-ph.IM].

[57] I. Mandel, W. M. Farr, and J. R. Gair, MNRAS **486**, 1086 (2019), http://oup.prod.sis.lan/mnras/article-pdf/486/1/1086/28390969/stz896.pdf.

[58] S. Vitale, (2020), arXiv:2007.05579 [astro-ph.IM].

[59] B. Abbott *et al.*, "GWTC-2 Data Release: Sensitivity of Matched Filter Searches to Binary Black Hole Merger Populations," (2020).

[60] W. M. Farr, Research Notes of the AAS **3**, 66 (2019).

[61] B. Abbott *et al.*, "GWTC-2 Data Release: Parameter Estimation Samples and Skymaps," (2020).

[62] J. S. Speagle, MNRAS **493**, 3132 (2020), https://academic.oup.com/mnras/article-pdf/493/3/3132/32890730/staa278.pdf.

[63] C. Talbot, R. Smith, E. Thrane, and G. B. Poole, Phys. Rev. D **100**, 043030 (2019).

[64] S. Husa, S. Khan, M. Hannam, P. Michael, F. Ohme, X. Jiméz Forteza, and A. Bohé, Phys. Rev. D **93**, 044006 (2016), arXiv:1508.07250 [gr-qc].

[65] M. Hannam, P. Schmidt, A. Bohé, L. Haegel, S. Husa, F. Ohme, G. Pratten, and M. Pürrer, Phys. Rev. Lett. **113**, 151101 (2014).

[66] S. Khan, S. Husa, M. Hannam, F. Ohme, P. Michael, X. Jiméz Forteza, and A. Bohé, Phys. Rev. D , 044007 (2016), arXiv:1508.07253 [gr-qc].

[67] S. Babak, A. Taracchini, and A. Buonanno, Phys. Rev. D **95**, 024010 (2017), arXiv:1607.05661 [gr-qc].

[68] A. Taracchini *et al.*, Phys. Rev. D **89**, 061502 (2014), arXiv:1311.2544 [gr-qc].

[69] Y. Pan, A. Buonanno, A. Taracchini, L. E. Kidder, M. H., H. P. Pfeiffer, M. A. Scheel, and B. Szilái, Phys. Rev. D **89**, 084006 (2014), arXiv:1307.6232 [gr-qc].

[70] B. Abbott *et al.* (LIGO Scientific, Virgo), Phys. Rev. Lett. **119**, 161101 (2017), arXiv:1710.05832 [gr-qc].

[71] B. Abbott *et al.* (LIGO Scientific, Virgo), Phys. Rev. Lett. **116**, 241102 (2016), arXiv:1602.03840 [gr-qc].

[72] C. Hoy and V. Raymond, (2020), arXiv:2006.06639 [astro-ph.IM].